Soil Dynamics and Earthquake Engineering 136 (2020) 106215

Contents lists available at ScienceDirect

Soil Dynamics and Earthquake Engineering

journal homepage: http://www.elsevier.com/locate/soildyn

Insights on nonlinear soil behavior and its variation with time at strong-motion stations during the Mw7.8 Kaikōura, New Zealand earthquake

Ying Zhou, Hongwei Wang, Ruizhi Wen *, Yefei Ren, Kun Ji

Key Laboratory of Earthquake Engineering and Engineering Vibration, Institute of Engineering Mechanics, China Earthquake Administration, No. 29 Xuefu Road, Harbin, Heilongjiang, 150080, People's Republic of China

A R T I C L E I N F O

Keywords:
Nonlinear soil behavior
Site response
Seismic ground motion
Predominant frequency
Recovery process

A B S T R A C T

To the end of investigating the potential nonlinear soil behavior at 44 strong motion stations during the 2016 M_w7.8 Kaikōura, New Zealand earthquake, we analyzed the modifications of the site response under the strong mainshock recording based on the horizontal-to-vertical spectra ratio, including the shift of the predominant frequency, and three nonlinearity indicators, DNL, ADNL, and PNL. Significant modifications to site response were observed at more than half of the stations, where the predominant frequency generally shifted to the lower one, and the DNL, ADNL, and PNL values were generally greater than 4.0, 0.3, and 10%, respectively. The strain proxy represented by PGV/V_{s30} was found in high level as the nonlinearity indicators were high. The deformation proxy may be a better indicator predicting the nonlinear soil behavior at sites with available shear-wave velocity. After the nonlinear soil behavior occurred, the soil structure completely recovered and the nonlinearity vanished after a period of time. The recovery process was dependent on the ground motion intensity immediately after the strong ground shaking, and the soil condition.

1. Introduction

Seismic ground motion was significantly affected by the superficial soil layers. It was well recognized that the amplifications generally for sedimentary sites on ground motion can be apparently different during the strong and weak ground shaking. Therefore, the nonlinear site term was persistently considered for the reliable prediction of ground motion [1]. Various peak ground accelerations (PGAs), e.g., 100–200 cm/s^2 [2], ~60 cm/s^2 [3], 35 cm/s^2 [4], 50 cm/s^2 downhole sensor [5] have been reported as the threshold value of PGA for indicating soil nonlinearity. The strong shaking drove the occurrence of the soil nonlinearity, especially for the superficial soil layers [5–7], i.e., a degradation of the soil shear modulus and an increase of the soil damping. Consequently, the nonlinear soil behavior on site response was generally characterized by the shifting of the predominant frequency to the lower frequencies and a reduction of the associated amplification.

The well recorded ground motions were extensively adopted to interpret the occurrence of the soil nonlinearity and its time-lapse changes. The site response curves between weak and strong ground shaking were directly compared to detect whether the soil nonlinearity occurred or not. In general, the site response was obtained using either the surface-to-borehole spectral ratio or the horizontal-to-vertical spectral ratio [8]. The nonlinear soil behavior has been widely observed by the drop of the predominant frequency [9–11] and the reduction of the amplification on the site response [10,12,13]. Moreover, references [5,14–16] proposed several parameters, which describe quantitatively the overall modification of the site response curves during the strong ground shaking, to characterize the effects of nonlinear soil behavior on site responses and further predict the soil nonlinearity. For observing the site nonlinear response under different level of seismic loading, the strain-stress relationship and the reduction of the shear modulus were examined according to the variation of the seismic velocity obtained by the cross-correlation analysis and seismic interferometry of the observed recordings from the vertical seismic array, and the auto-correlation analysis of seismic waveforms at a single station [17–22]. In these studies, the peak ground acceleration (PGA) and the

* Corresponding author. Key Laboratory of Earthquake Engineering and Engineering Vibration, Institute of Engineering Mechanics, China Earthquake Administration, No. 29 Xuefu Road, Harbin, Heilongjiang, 150080, People's Republic of China.

E-mail addresses: joey052zy@163.com (Y. Zhou), whw1990413@163.com (H. Wang), ruizhi@iem.net.cn (R. Wen), renyefei@iem.net.cn (Y. Ren), jikun@iem.ac.cn (K. Ji).

https://doi.org/10.1016/j.soildyn.2020.106215
Received 1 December 2019; Received in revised form 26 March 2020; Accepted 4 May 2020

ratio between the peak ground velocity (PGV) and the equivalent shear-wave velocity (V_s) were assumed to be proxies of shear stress and strain, respectively. Compared with the incident ground motion intensity, the deformation proxy, PGV/V_s, was proved to be a good representation for predicting the nonlinear soil behavior [18–20].

On November 14, 2016, an M_W7.8 great earthquake with epicentre at Kaikōura shook the north Canterbury. Post-earthquake geodetic and field surveys identified the widespread and devastating ground damages by landslides, active faults, and crustal shift, etc [23–25]. The extremely strong ground motions were reported and recorded by the strong-motion observation stations of GeoNet [26], and were responsible for the damages to many structures and infrastructure [26–28]. Several stations recorded the peak ground acceleration (PGA) over 1.0 g (g, gravity acceleration), and a total of 44 stations recorded the horizontal PGA (i.e., geometrical mean of PGAs at both horizontal components) greater than 100 cm/s^2. According to the GeoNet database of site metadata [29], these stations were classified into four classes defined by the New Zealand design standard NZS1170.5, comprising 10 class-B sites (soft rock), 5 class-C sites (shallow soil), 26 class D sites (deeper or soft soil), and 3 class-E sites (very soft soil). According to the quality assessment [29], a total of 11 out of 44 stations were assumed to have credible V_{s30} values with approximate uncertainties of <20%. The V_{s30} values for these stations were in the range of 120–274 m/s, indicating the soft soil site. Until 1 March 2017, a total of 367 Kaikōura aftershocks with M_L = 4.00–6.26 were recorded by the strong-motion stations of GeoNet and over 12,000 three-component acceleration recordings were collected.

In order to examine the occurrence of nonlinear soil behavior and its time-laspe changes at the 44 stations recorded the horizontal PGA greater than 100 cm/s^2 during the Kaikōura earthquake, the modifications of site responses under strong ground motions were evaluated by the shift of the predominant frequency and several quantitative parameters, including degree of nonlinearity (DNL), absolute degree of nonlinearity (ADNL), and percentage of nonlinearity (PNL). The S-wave horizontal-to-vertical (H/V) spectral ratio was used approximately as the site response, and the reference site response under weak ground motions was represented by the mean of the H/V spectral ratios over recordings with PGA smaller than 10 cm/s^2. As demonstrated by Wen [8] and Régnier [5], the nonlinear site responses can be evaluated using the H/V spectral ratios.

2. Datasets and data processing

GeoNet, established in 2001, is the result of a partnership between the EQC as investment manager and GNS Science as technical manager. It uses a network of over 600 sensors spread across New Zealand to detect, analyse, and respond to natural hazards as they happen in order to deliver a modern geological hazard monitoring system for New Zealand. A total of 160 strong-motion stations of GeoNet recorded the M_W7.8 Kaikōura earthquake. From 13 November 2016 to 1 March 2017, 12,313 strong-motion recordings were collected at 264 stations in 367 Kaikōura aftershocks with M_L = 4.00–6.26. A total of 44 stations which recorded the horizontal PGA greater than 100 cm/s^2 during the Kaikōura mainshock were considered in this study, as shown in Fig. 1 and listed in Table 1. Up until 1 March 2017, 2992 recordings with hypocentral distances (R) smaller than 200 km were obtained by the 44 stations during the Kaikōura aftershocks. The horizontal PGAs of recordings at these stations were plotted against earthquake-to-station distance in Fig. 2. The Joyner-Boore distance (R_{JB}) and hypocentral distance were used as the earthquake-to-station distance for recordings from the mainshock and aftershocks, respectively. The R_{JB} values of the mainshock recordings were directly derived from the New Zealand strong-motion database flatfile (https://static.geonet.org.nz/info/resources/applications_data/earthquake/strong_motion/Flatfiles.zip). The horizontal PGAs were not greater than 10 cm/s^2 for most aftershock recordings and fell in the range of 100–200 cm/s^2 for most mainshock recordings.

These recordings were first processed by baseline correction and a Butterworth bandpass filter. The high-cut corner frequency was uniformly set to 25 Hz, while the magnitude-dependent low-cut corner frequency f_{lc} was adopted, i.e., 0.25 Hz for M_L<4.5, 0.2 Hz for M_L = 4.5–5.0, 0.15 Hz for M_L = 5.0–5.5, and 0.1 Hz for M_L≥5.5. The S waves were extracted according to the Husid function [30] and the cumulative root-mean-square (RMS) function [31]. Cosine tapers were added at the beginning and end of the extracted S wave to eliminate truncation effects, and the length of each taper was 10% of the S-wave window length [32–35]. In order to guarantee the spectral resolution, the minimum length of the S-wave window was not less than 1.0/1.25 f_{lc}. The Fourier amplitude spectra of the S wave were calculated and smoothed using the windowing function [36] with b = 20. The H/V spectral ratios [37] were calculated using the S-wave amplitude spectra at frequencies with

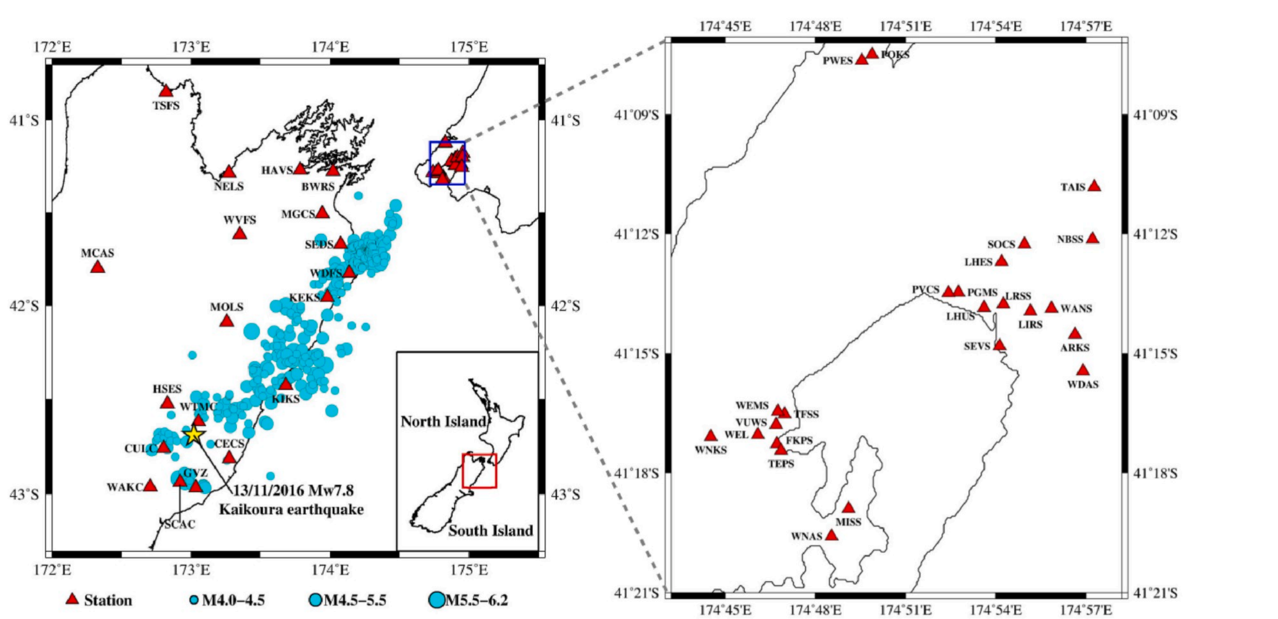

Fig. 1. Locations of earthquakes (cyan circles) and strong-motion stations (red triangles) considered in this study. Yellow star indicates the epicentres of the 2016 M_W7.8 Kaikōura earthquake. (For interpretation of the references to color in this figure legend, the reader is referred to the Web version of this article.)

Table 1
Site conditions and calculated nonlinear site indicators at 44 strong motion stations.

Site Code	Site Class	Number of weak records	Horizontal PGA (cm/ s^2)	V_{S30}	V_{S30} quality assessment	T_{site}	T_{site} quality assessment	DNL	ADNL	PNL (%)	F_p (Hz) of Mainshock	F_p (Hz) of Weak ground motions	S. D. ($\log_{10}$)	Potential nonlinear soil bahavior
ARKS	C	26	232	270	Q_3	0.33	Q_1	2.74	0.23	16.79	1.72	2.49	0.048	Non
BWRS	B	141	136	760	Q_3	0.2	Q_1	3.98	0.24	9.21	3.65	4.57	0.064	Non
CECS	D	120	277	270	Q_3	2.2	Q_3	4.07	0.19	7.93	–	–	–	Yes
CULC	D	47	232	270	Q_3	1.2	Q_3	6.41	0.4	8.63	–	–	–	Yes
FKPS	D	22	149	250	Q_3	0.9	Q_2	5.27	0.41	13.17	–	–	–	Yes
GVZ	B	97	126	1000	Q_3	–	Q_3	3.67	0.12	2.9	–	–	–	Non
HAVS	B	119	111	1000	Q_3	–	Q_3	1.87	0.06	2.18	5.71	6.03	0.064	Non
HSES	D	105	246	280	Q_3	0.9	Q_1	5.21	0.31	16.16	0.78	1.43	0.039	Yes
KEKS	B	122	978	1000	Q_3	–	Q_3	1.84	0.21	16.92	1.51	2.14	0.117	Non
KIKS	B	101	218	1000	Q_3	–	Q_2	3.52	0.12	4.66	–	–	–	Non
LHES	D	12	157	240	Q_3	1.16	Q_3	7.94	0.58	13	–	–	–	Yes
LHUS	D	38	140	212	Q_1	2	Q_3	9.14	0.8	22.39	–	–	–	Yes
LIRS	C	20	98	400	Q_3	0.25	Q_1	2.76	0.18	7.08	1.4	3.73	0.065	Non
LRSS	D	38	155	230	Q_3	1.4	Q_3	9.14	0.99	35.54	0.48	0.59	0.123	Yes
MCAS	D	40	112	501	Q_3	1.6	Q_3	5.08	0.26	9.6	0.53	0.49	0.121	Yes
MGCS	E	29	227	150	Q_3	1	Q_3	6.36	0.41	12.43	1.94	3.8	0.099	Yes
MISS	D	86	161	200	Q_1	1	Q_1	2.8	0.37	29.21	0.67	0.93	0.202	Yes
MOLS	C	127	292	700	Q_3	0.2	Q_2	2.24	0.03	2.33	4.49	5.5	0.606	Non
NBSS	E	50	206	190	Q_1	0.9	Q_1	9.26	0.91	29.24	0.81	1.02	0.088	Yes
NELS	B	48	114	1000	Q_3	0.8	Q_2	2.43	0.07	2.1	1.57	1.78	0.551	Non
PGMS	D	40	134	200	Q_2	2	Q_2	8.96	0.75	14.66	0.44	0.54	0.086	Yes
POKS	C	32	100	330	Q_3	0.25	Q_2	7.99	0.51	12.4	3.34	4.74	0.086	Yes
PVCS	D	29	166	190	Q_2	2	Q_3	7.76	0.66	12.75	0.44	0.54	0.067	Yes
PWES	B	95	97	1000	Q_3	–	Q_3	6.43	0.42	9.33	–	–	–	Yes
QCCS	D	10	236	270	Q_3	0.28	Q_1	3.5	0.27	16.94	2.78	3.73	0.022	Non
SCAC	D	26	259	270	Q_3	0.9	Q_2	4.71	0.25	8.42	1.82	2.03	0.455	Yes
SEDS	D	87	666	270	Q_3	1	Q_3	3.6	0.13	7.9	–	–	–	Non
SEVS	D	37	183	210	Q_3	1.1	Q_2	6.87	0.76	35.69	0.72	0.78	0.126	Yes
SOCS	D	13	148	300	Q_3	1.2	Q_3	6.86	0.5	11.02	–	–	–	Yes
TAIS	D	50	132	250	Q_3	0.6	Q_2	9.75	0.86	24.11	1.35	1.43	0.214	Yes
TEPS	D	85	154	267	Q_1	1.2	Q_1	3.42	0.35	30.34	0.66	1.06	0.177	Yes
TFSS	D	22	174	274	Q_1	1.3	Q_2	6.51	0.55	20	–	–	–	Yes
TSFS	B	10	103	1000	Q_3	0.38	Q_2	2.78	0.23	12.58	2.53	3.1	0.028	Non
VUWS	D	34	196	250	Q_2	0.8	Q_2	5.73	0.45	11.2	–	–	–	Yes
WAKC	D	92	145	270	Q_3	0.8	Q_3	4.14	0.18	6.61	1.6	1.66	0.448	Yes
WANS	B	24	127	1000	Q_3	0.2	Q_2	2.68	0.11	6.05	4.74	5.2	0.043	Non
WDAS	E	58	161	120	Q_1	1.6	Q_2	7.97	0.87	25.73	0.78	0.78	0.034	Yes
WDFS	D	86	1008	270	Q_3	70	Q_3	3.18	0.12	7.88	–	–	–	Non
WEL	B	90	133	1000	Q_3	0.3	Q_1	3.83	0.26	9.08	3.13	3.34	0.106	Non
WEMS	D	89	135	265	Q_1	0.8	Q_2	7.48	0.54	13.97	0.55	1.17	0.443	Yes
WNAS	D	40	130	239	Q_2	0.78	Q_2	4.31	0.34	13.02	1.35	1.54	0.047	Yes
WNKS	C	55	179	270	Q_3	0.38	Q_1	5.84	0.46	17.8	2.18	2.63	0.029	Yes
WTMC	D	40	890	210	Q_3	0.6	Q_3	8.54	0.71	36.56	–	–	–	Yes
WVFS	D	20	153	270	Q_3	0.7	Q_2	6.28	0.41	10.07	1.82	2.07	0.155	Yes

signal-to-noise ratio greater than 5.0. Here, the pre-P wave noise windows with the same length of the S-wave window were extracted and their Fourier amplitude spectra were provided for the calculation of signal-to-noise ratio. An example illustrating how to extract S-wave window and determine the useable frequency band was shown in Fig. 3.

3. Shifting of the predominant frequency

Fig. 4 shows the reference site response, i.e., the average of the S-wave H/V spectral ratios for recordings with PGA smaller than 10 cm/s^2, and its uncertainty represented by the one standard deviation range. The site predominant frequency was identified from the reference site response, and its uncertainty was described by the standard deviation of the predominant periods of the S-wave H/V spectral ratio curve for individual recording with PGA<10 cm/s^2, as shown in Fig. 4 and listed in Table 1. Noted that the site predominant frequency was difficult to identify from the flat reference site response, e.g., stations CECS, CULC, WTMC, etc. The H/V spectral ratio curve of recording of Kaikōura mainshock with horizontal PGA greater than 100 cm/s^2 was plotted in Fig. 4 for comparison with the reference site response.

Kaiser [29] provided the fundamental site period (T_{site}) in the GeoNet database of site metadata. According to the quality assessment of the measured T_{site}, stations were classified into three categories, i.e., Q_1, Q_2, and Q_3 which represent the approximate uncertainty of <10%, 10–20%, and >20%, respectively. The predominant frequency identified from reference site response were compared with that inferred from the provided T_{site}, as shown in Fig. 5(a). In order to avoid the effect of bad-quality T_{site} as much as possible, 23 stations with T_{site} values within Q_1 and Q_2 categories were adopted for comparison. Our results identified from the reference site response were in good agreement with those inferred from the T_{site} for 10 Q_1 stations. Our results and the inferred results did not show significant differences for the remaining 13 Q_2 stations, although the discrepancies were much greater than those Q_1 stations. The comparison indicated that the predominant frequency identified from the reference site response was credible. Furthermore, the predominant frequencies identified respectively from the reference site response and the H/V spectral ratio curve under the mainshock were compared and plotted in Fig. 5(b). It was clearly found that almost all dots in this figure were above a 1:1 line, which indicated that the predominant frequency under strong ground motion shifts to the lower frequency from a higher frequency under weak ground motion.

Station WTMC was located very close to the epicentre and the R_{JB} was equal to 0 km. The horizontal PGA was over 1.0 g, the strongest in the mainshock. The reference site response approximately flat over a

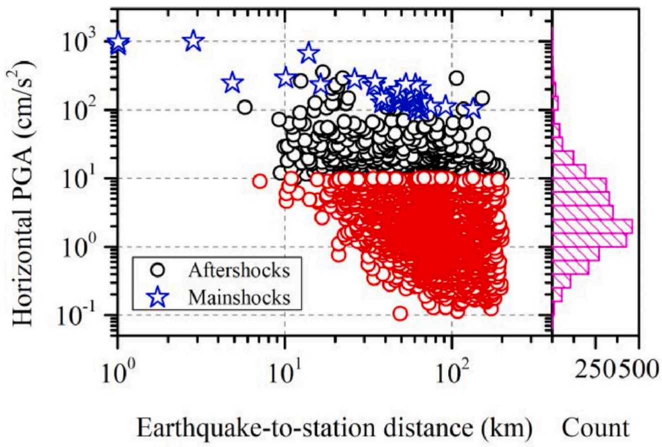

Fig. 2. Horizontal peak ground acceleartions (PGAs) versus the earthquake-to-station distance for recordings obtained at 44 stations considered in this study in the Kaikoura seismic sequence up until 1 March 2017. The horizontal PGA was represented by the geometrical mean of PGAs at both horizontal components (East-West and North-South). The earthquake-to-station distance was represented by the Joyner-Boore distance for the mainshock recordings (stars) and hypocentral distance for the aftershocks (circles), respectively. PGAs observed at two stations with Rjb = 0 km in the kaikoura earthquake are plotted on the vertical axis (i.e., Rjb = 1 km).

wide frequency band of 0.5–10.0 Hz and it was very difficult for us to identify the site predominant frequency. However, the clear predominant frequency at ~0.7 Hz was observed from the H/V spectral ratio under the mainshock. Such observation indicated the strong reduction of the shear-wave velocity under the strong ground motion. Moreover, the H/V spectral ratios using the moving time windows of the mainshock waveform were performed to observe the coseismic variation of the predominant frequency, as shown in Fig. 6(a). For comparison, the same was performed for a recording from an aftershock with weak ground motion (Fig. 6(b)). The predominant frequency rapidly went down to ~0.7 Hz as it experienced the strongest S wave during the Kaikōura mainshock, and then recovered to the higher level (~2Hz) immediately after the strong S wave. However, the predominant frequency, ~ did not show any apparent fluctuation as it experienced the weak ground motion in the aftershock.

4. Nonlinear soil behavior indicators

We further adopted three indicators to evaluate whether the nonlinear soil behavior occurred. The first indicator was DNL proposed firstly by Noguchi and Sasatani [38], which can be expressed as

$$DNL = \sum_{i=N_1}^{N_2} \left| \log\left(\frac{HVSR_{strong}(i)}{HVSR_{weak}(i)}\right) \right| (f_{i+1} - f_i), \tag{1}$$

where $HVSR_{strong}(i)$ is the S wave H/V spectral ratio value at frequency f_i under strong ground motion, $HVSR_{weak}(i)$ is the reference site response at frequency f_i. N_1 and N_2 are the first and last frequency points, respectively. The second indicator was ADNL proposed by Ren [16], which can be expressed as

$$ADNL = \sum_{i=N_1}^{N_2} \delta(i) \cdot [\log(f_{i+1}) - \log(f_i)], \tag{2}$$

$$\delta(i) = \begin{cases} \log(HVSR_{strong}(i)) - \log(HVSR^{+}_{weak}(i)) & HVSR_{strong}(i) \geq HVSR^{+}_{weak}(i) \\ \log(HVSR^{-}_{weak}(i)) - \log(HVSR_{strong}(i)) & HVSR_{strong}(i) \leq HVSR^{+}_{weak}(i), \\ 0 & \text{others} \end{cases} \tag{3}$$

where $HVSR^{+}_{weak}(i)$ and $HVSR^{-}_{weak}(i)$ represent the average H/V spectral ratio of weak ground motions plus and minus one standard deviation, respectively. The third indicator was PNL proposed by Regnier [5],

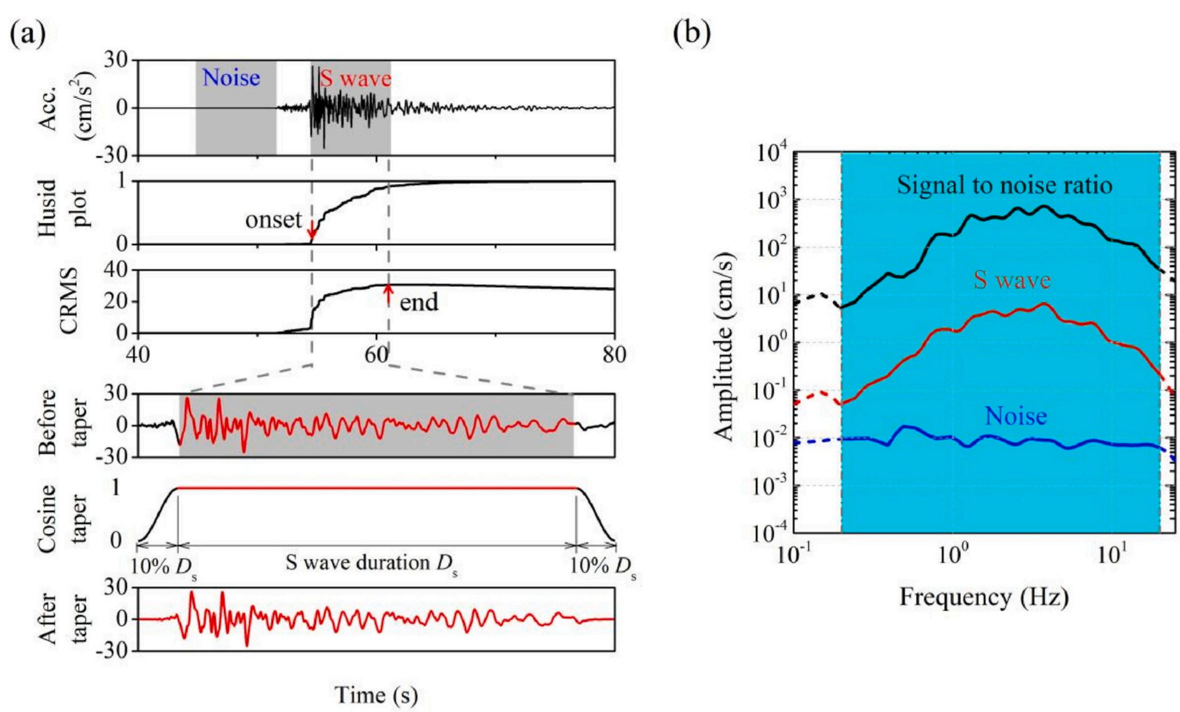

Fig. 3. (a) Illustration of how to extract and process S-wave window. **(b)** the Fourier amplitude spectra for the extracted S wave (red solid line) and the pre-P wave noise window (blue solid line), and calculated signal-to-noise ratio (black solid line). The shaded area indicates the useable frequency band determined according to the signal-to-noise ratio and low-cut corner frequency. (For interpretation of the references to color in this figure legend, the reader is referred to the Web version of this article.)

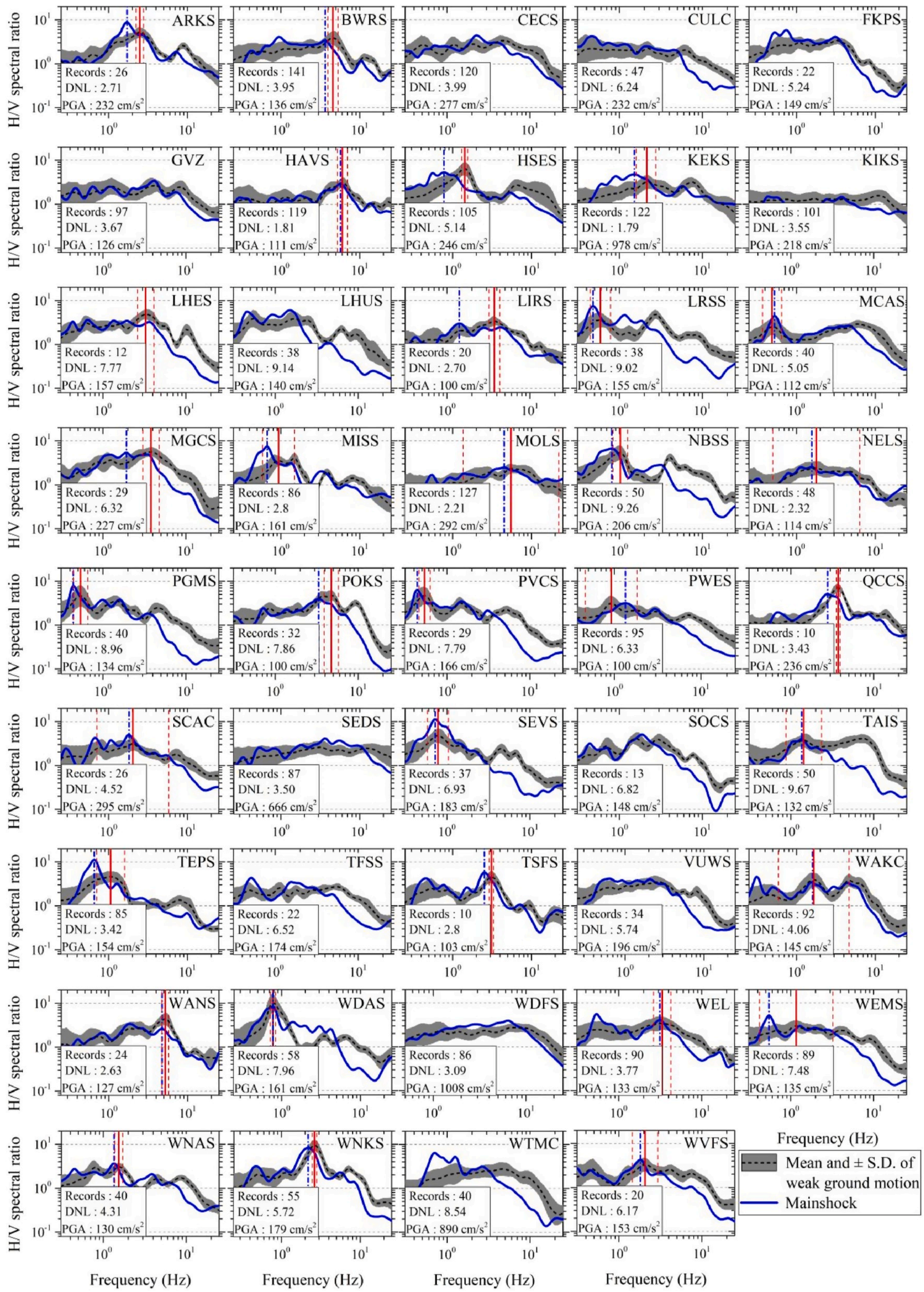

Fig. 4. The reference site response (black dashed line) and its uncertainty (shaded area) represented by the average and one standard deviation range of the S-wave horizontal-to-vertical (H/V) spectral ratios using the recordings with horizontal peak ground acceleration (PGA) smaller than 10 cm/s^2, respectively. Blue solid line represents the H/V spectral ratio curve of the recording from 2016 Kaikōura mainshock with horizontal PGA greater than 100 cm/s^2. The predominant site period wes identified from the reference site response and drawn in red solid line, and the red dashed line represents its uncertainty. The blue dashed-dotted line indicats the predominant frequency identified from the H/V spectral ratio curve of the mainshock recording. The number of recordings used for the calculation of reference site response, the PGA values of the mainshock recording and the calculated degree of nonlinearity (DNL) were also shown. (For interpretation of the references to color in this figure legend, the reader is referred to the Web version of this article.)

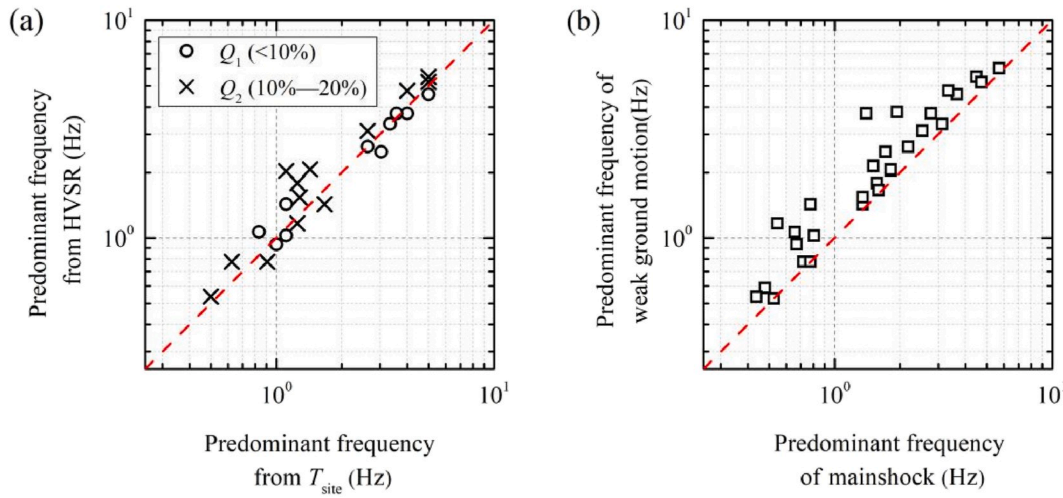

Fig. 5. (a) Comparison of the predominant site frequency identified from the reference site response and inferred from the Tsite values reported by Kaiser et al. (2017) for 23 stations with quality assessment of T_{site} equal to Q_1 and Q_2. (b) Comparison of the predominant frequency identified from the reference site response under weak ground motion and horizontal-to-vertical spectra ratio curve under mainshock.

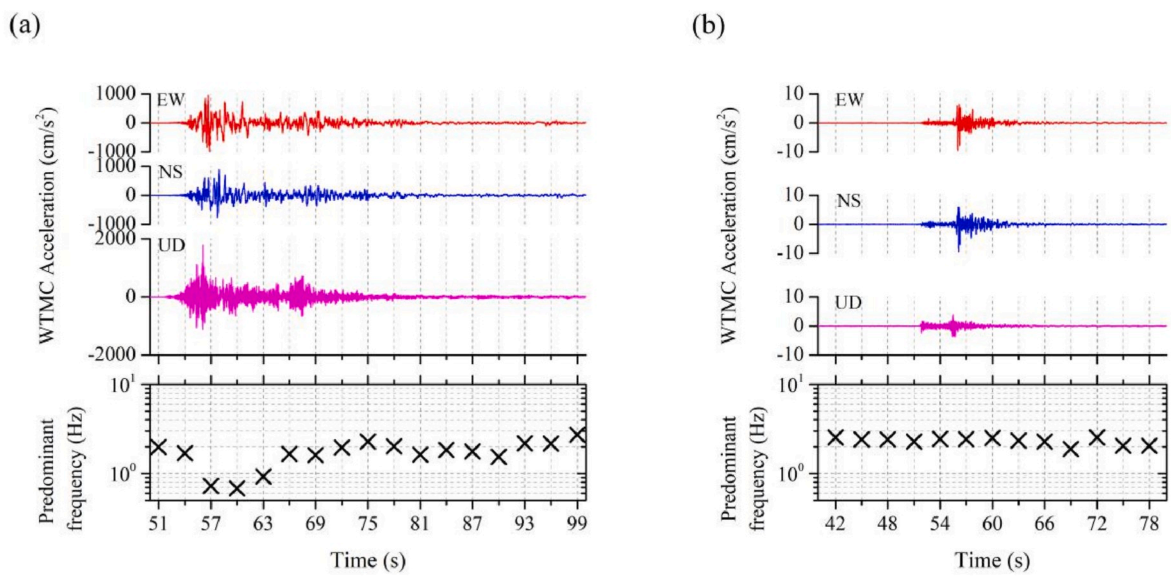

Fig. 6. The acceleration waveforms recorded at station WTMC during the **(a)** 2016 Kaikōura mainshock and **(b)** an aftershock. Crosses indicate the predominant frequencies identified from the horizontal-to-vertical spectral ratio curve using the moving windows.

which can be expressed as:

$$A=\begin{cases}\left(\mathrm{HVSR}_{strong}(i)-\mathrm{HVSR}^{+}_{weak}(i)\right)\log\left(\dfrac{f_{i+1}}{f_i}\right) & \mathrm{HVSR}_{strong}(i)\geq\mathrm{HVSR}^{+}_{weak}(i)\\ \left(\mathrm{HVSR}^{-}_{weak}(i)-\mathrm{HVSR}_{strong}(i)\right)\log\left(\dfrac{f_{i+1}}{f_i}\right) & \mathrm{HVSR}_{strong}(i)\leq\mathrm{HVSR}^{+}_{weak}(i)\\ 0 & \text{others}\end{cases}, \tag{4}$$

$$\mathrm{PNL}=100\frac{A}{\sum\limits_{i=N_1}^{N_2}\mathrm{HVSR}_{weak}(i)\cdot[\log(f_{i+1})-\log(f_i)]}. \tag{5}$$

Fig. 7 provided an illustration for the calculation of the three indicators. The three indicators calculated were listed in Table 1.

The three indicators calculated were listed in Table 1 and plotted in Fig. 8. As reported by Ref. [5,11,38], a DNL indicator over 4 indicates the potential occurrence of the nonlinear soil behavior. After evaluating the nonlinear soil behavior during the 2008 great Wenchuan earthquake, Ren [16] proposed the thresholds of DNL, ADNL, and PNL, which were equal to 4.0, 0.2, and 7%, respectively. In our study, the calculated DNL values were mainly in the range of ∼2–∼10, and high DNL values greater than 4 were found at 27 stations. It was found that both the ADNL and the PNL correlated well with the DNL. Both indicators showed the upward tendency as the DNL increased. For the 27 stations with DNL>4, the ANDL and PNL values were, in general, greater than 0.3 and 10.0%, respectively.

The deformation proxy, PGV/V_s, was commonly used to interpret the nonlinear soil behavior. The threshold values of the strain indicating the hysteretic nonlinear behavior with permanent deformation was found to be $\sim10^{-4}$ or 2×10^{-4} by many previous studies [39–42]. The same as T_{site}, Kaiser [29] provided the quality assessment of V_{s30} for the GeoNet stations, i.e., Q_1, Q_2, and Q_3 with uncertainties <10%, 10–20%, and >20%, respectively. Fig. 9 plotted these calculated indicators against the corresponding deformation proxies, PGV/V_{s30}, for 11 stations (highlighted in Fig. 8) with credible V_{s30} values (Q_1 and Q_2). The V_{s30} values

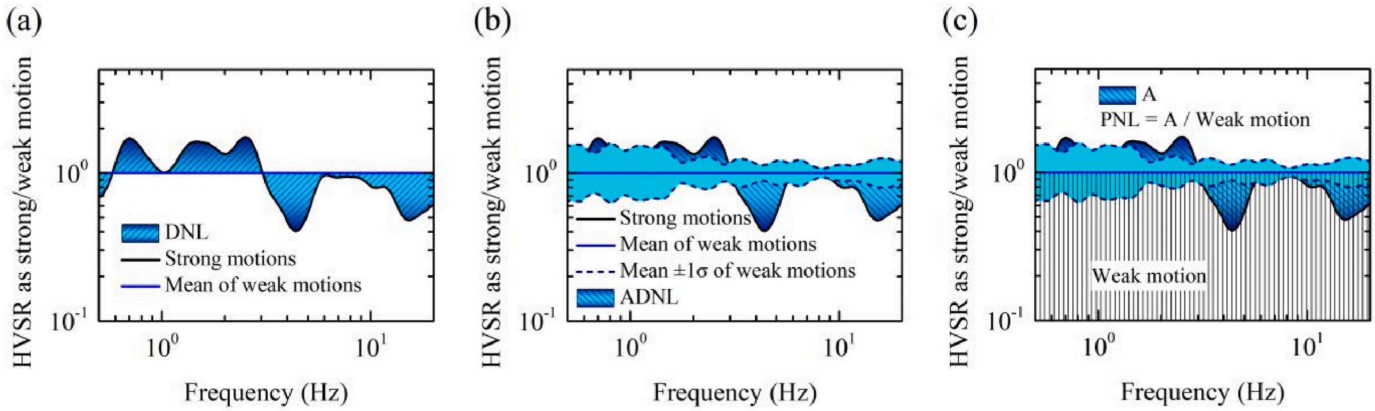

Fig. 7. Illustration of the calculation of **(a)** DNL, **(b)** ADNL, and **(c)** PNL using site QCCS as an example.

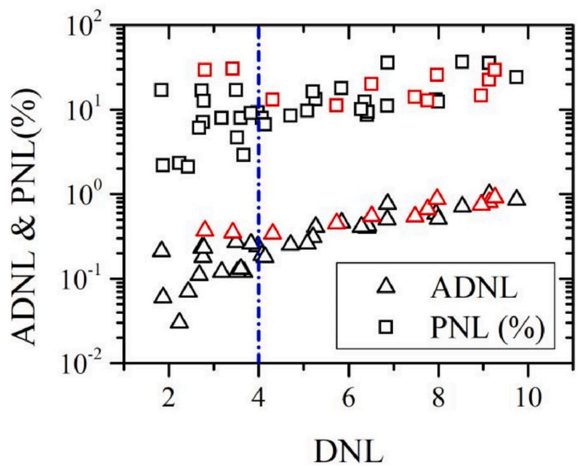

Fig. 8. The nonlinearity indicators DNL, ADNL, and PNL calculated for the 44 stations considered in this study. The red squares or triangles represent the 11 stations with credible V_{s30} values (Q_1 and Q_2). (For interpretation of the references to color in this figure legend, the reader is referred to the Web version of this article.)

for the 11 stations were in the range of 120–274 m/s, indicating the soft soil sites. The small strain values, i.e., PGV/V_{s30} = 3×10^{-7}-3×10^{-4} were observed for the cases that the PGA values of recordings were not greater than 50 cm/s^2. Correspondingly, the calculated DNL, ADNL, and PNL indicators did not show strong variation with the increase of the strain values and the mean values were respectively equal to 2.0, 0.08, and 4.0%, although the large scatters were observed due to the uncertainty of the site response derived from the H/V spectral ratio of single recording. As the PGA increased and reached up to 100 cm/s^2, the PGV/V_{s30} values generally greater than 10^{-3} depict the high strain. Meanwhile, the much higher DNL, ADNL, and PNL parameters were observed for these stations, except that DNL indicator for two stations were smaller than 4. In view of the high DNL, ADNL, PNL, and the deformation proxies, it is more likely that the nonlinear soil behavior occurred at the 11 stations considered during the strong ground shaking with PGA>100 cm/s^2. Although the deformation proxies were not available due to the incredible V_{s30} measures (Q_3) for the remaining 33 stations, we preliminarily judged that nonlinear soil behavior was more likely occur at those stations with DNL>4.

5. Variation of site nonlinearity with time

Ten out of the 44 stations were selected to examine the time-lapse change of the nonlinear soil behavior, highlighted in Table 1. The

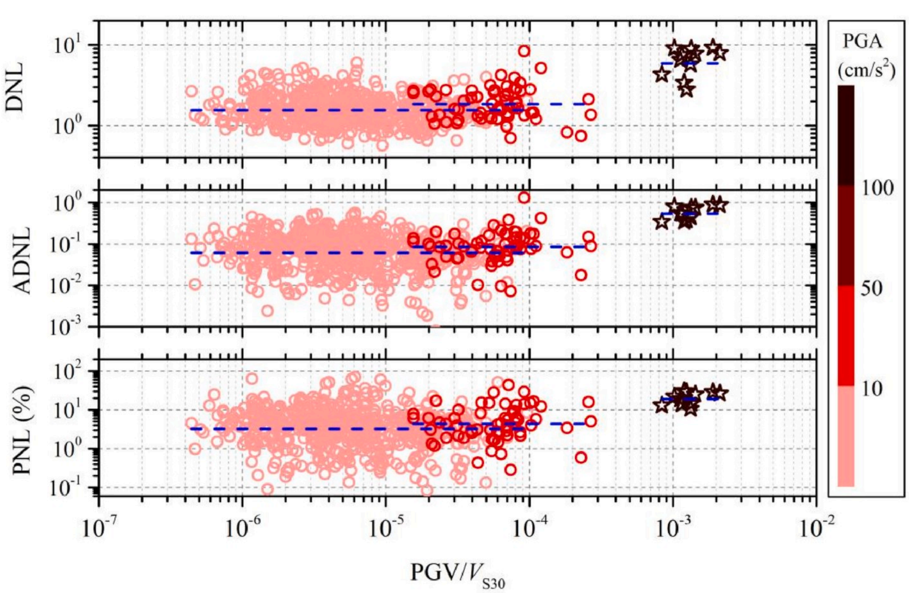

Fig. 9. The calculated DNL, ADNL, and PNL parameters at stations classified into categories Q1 and Q2 versus the strain proxies assumed to be the ratio between the peak ground velocity and the time-weighted average shear-wave velocity over the upper 30 m (PGV/V_{S30}). The individual observed ground motion recordings were used for the calculations of these parameters according to the mean of the H/V spectral ratios of recordings with peak ground acceleration (PGA) smaller than 10 cm/s^2. Stars and circle represent the calculated parameters using recording from the Kaikoura mainshock and aftershocks, respectively. The color scales indicate the PGA values. (For interpretation of the references to color in this figure legend, the reader is referred to the Web version of this article.)

selected stations followed two conditions: (1) The station obtained at least 5 weak recordings with PGA smaller than 10 cm/s^2 within 10 months before the Kaikōura earthquake; (2) The credible T_{site} values (Q_1 and Q_2) can be obtained, and the predominant frequency can be well identified from the H/V spectral ratio curve. For the selected ten stations, the predominant frequencies were identified from the H/V spectral ratio curves of individual recording before and after the mainshock, and the DNL, ADNL, and PNL indicators were calculated for recordings with PGA greater than 10 cm/s^2. Fig. 10 provided the identified predominant frequency and the calculated indicators varied with time for four typical stations, HSES, TAIS, WNKS, and NBSS (see Fig. 11).

When the Kaikōura mainshock occurred, the horizontal PGA achieved 250 cm/s^2 at station HSES, the predominant frequency suddenly dropped to 0.78 Hz. The high DNL, ADNL, and PNL values were obtained, equal to 5.21, 0.31 and 16.16%, respectively. Significant difference between the H/V spectral curve of the mainshock recording and the reference site response, indicated by the predominant frequency and several indicators, revealed the occurrence of the nonlinear soil behavior at this station. Three aftershocks subsequently occurred at 28 s, 50 s, and 83 s after the mainshock, and the recorded PGAs at this station were 40 cm/s^2, 55 cm/s^2, and 60 cm/s^2, respectively. The identified predominant frequency, i.e., 0.91 Hz, 0.88 Hz, and 1.18 Hz, respectively, approximately showed an increasing tendency and gradually reached close to the identified result from the reference site response. Correspondingly, the calculated DNL, ADNL, and PNL values showed a gradually decreasing tendency. Following the three aftershocks, large numbers of aftershocks occurred and were recorded by the HSES station. The recorded horizontal PGA values were not greater than 10 cm/s^2, except for three at 13–24 h after the mainshock. The maximum horizontal PGA, which was recorded at about 13.5 hrs after the mainshock, reached up to 195 cm/s^2. Although this station suffered from strong ground motion again, the identified predominant frequency was very close to that from the reference site response and the calculated DNL, ADNL, and PNL indicators did not show high values, indicating that the nonlinear soil behavior did not occur again. Before the mainshock, a total of 11 weak recordings were obtained at HSES station. The identified predominant frequencies from the H/V spectral ratio curve of individual recording were mainly in the range of 1.32–1.71 Hz, approximately consistent with the identified predominant frequency (1.43 Hz) using the weak aftershock recordings, indicated that the soil

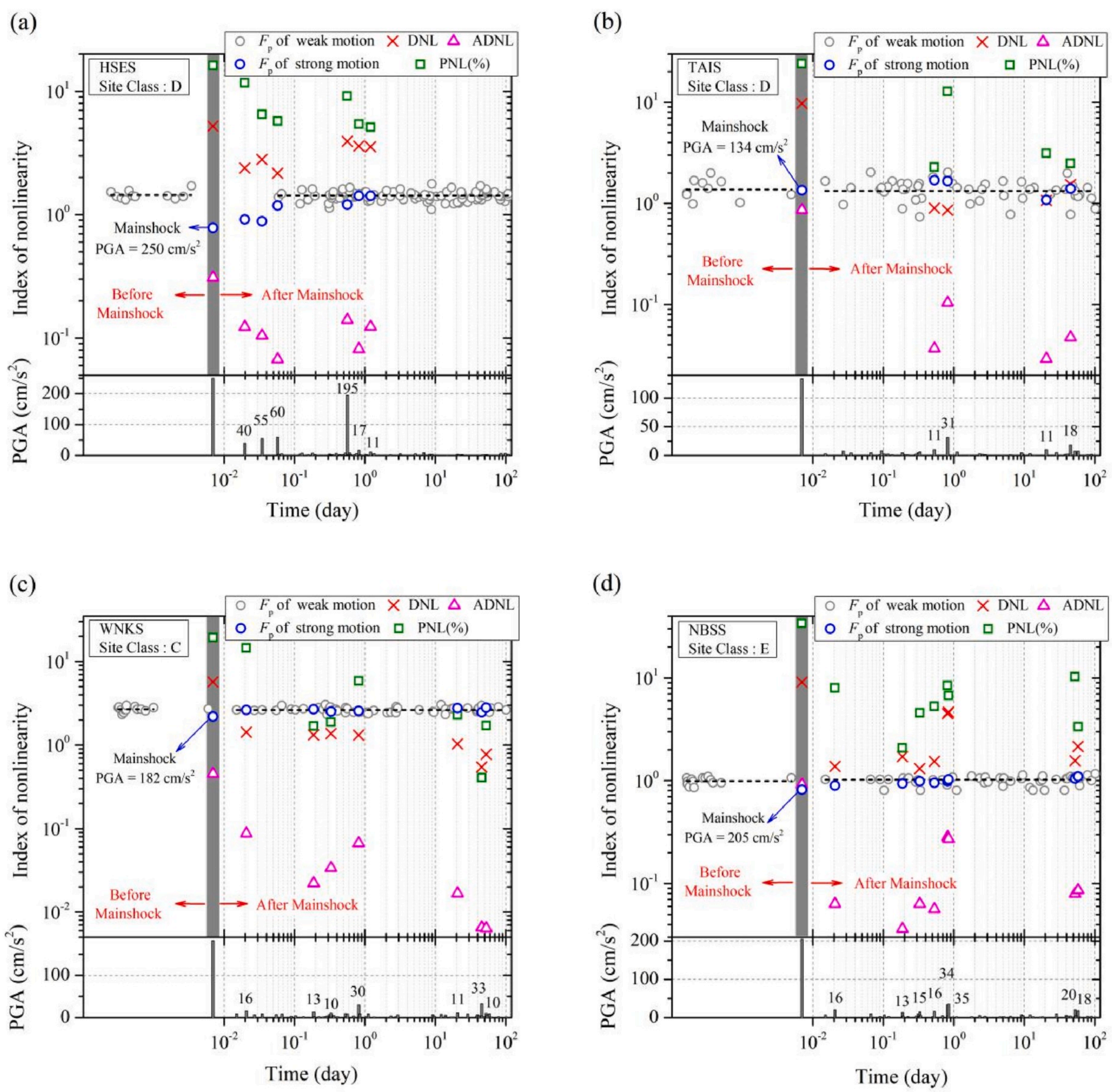

Fig. 10. The predominant frequencies and the nonlinearity indicators (DNL, ADNL, and PNL) varied with time for four typical stations HSES (a), TAIS (b), WNKS (c), and NBSS (d), respectively. The PGA values of recording from the Kaikoura mainshock and the following aftershoks were also plotted. The dashed bars indicate the time for the mainshock.

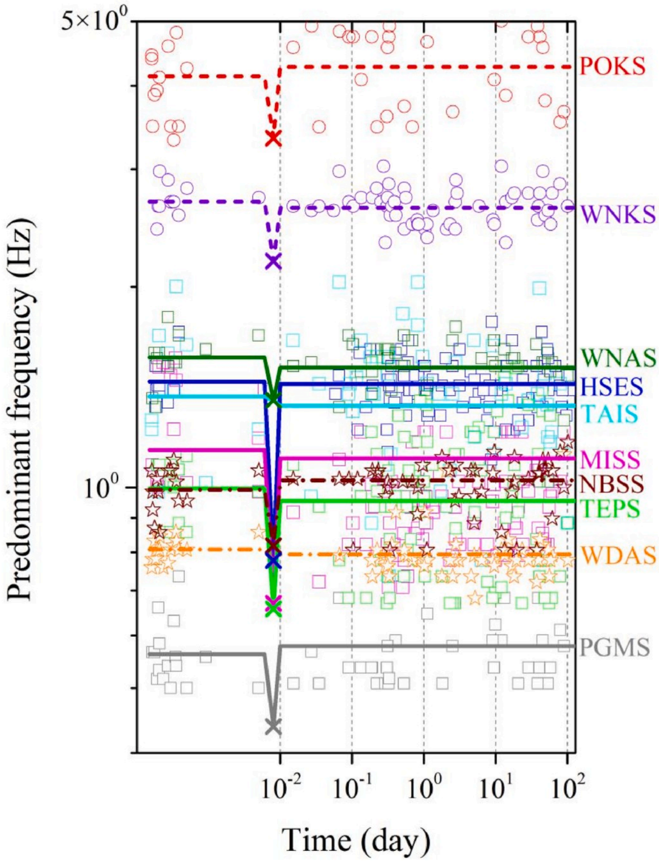

Fig. 11. The varied predominant frequency with time for the ten stations.

structure completely recovered from the nonlinear behavior after suffering from the strong Kaikōura mainshock. It should also be noted that the recovery from the nonlinear soli behavior was delayed by the relatively stronger PGAs immediately after the mainshock.

It was clearly observed that the reference site response of station TAIS has two peaks at 1.43 Hz and 7.50 Hz, respectively (shown in Fig. 4), which may be ascribed to two boundaries with high impendence contrast. The H/V spectral ratio curve of the mainshock recording with PGA equal to 134 cm/s^2 showed an apparent single peak, and the predominant frequency was identified to be 1.35 Hz approximately consistent with that of the reference site response. However, the high DNL, ADNL, and PNL indicators (Table 1) were observed, indicating the significant modification of the site response curve by the strong ground motion. We thus inferred that the vanishing peak at 7.50 Hz under the strong ground motion may be resulted from the decreased shear-wave velocity for one soil layer over or below any one boundary with high impedance contrast. The nonlinearity indicators were further considered to examine the variation of nonlinear soil behavior after the mainshock. The most PGAs recorded during the aftershocks were not greater than 10 cm/s^2, and the DNL, ADNL, and PNL indicators for four recordings with PGAs in the range of 10–50 cm/s^2 were calculated. These indicators for the four aftershock recordings were significantly smaller than those from the mainshock, e.g., DNLs = 1–2, indicating the complete recovery of soil structure from the strong ground motion during the mainshock.

As the same to the station TAIS, the predominant frequency was slightly lower than that of the reference site response during the strong mainshock at station WNKS, while the nonlinearity indicators, DNL, ADNL, and PNL decreased obviously after the mainshock compared with those during the mainshock. For example, the DNL values according to seven aftershock recordings with PGA mainly in the range of 10–30 cm/s^2, were found to be generally close to 1.0, significantly lower than 5.72 based on the mainshock. Such results indicated the disappearing of the nonlinear soil behavior after the strong ground motion at this station.

The reference site response of station NBSS also showed two peaks, and the lower frequency was identified as the predominant frequency. When the mainshock occurred, the predominant frequency at station NBSS slightly decreased to 0.82 Hz, meanwhile the high-frequency peak also slighted shifted from ~4.0 Hz to ~3.0Hz. However, the high values for the calculated DNL, ADNL, and PNL indicators were observed, i.e., 9.13, 0.92, and 34.12%, respectively. We focused on the nonlinearity indicators in eight aftershock recordings with PGA in the range of 13–35 cm/s^2. The NBSS stations recorded the relatively larger PGAs of 34–35 cm/s^2 about 20 hrs after the mainshock. This station also recorded another four PGAs around 15 cm/s^2 and two PGAs around 20 cm/s^2 before and after the larger PGAs, respectively. We noted that the nonlinearity indicators from two larger PGAs, 34 and 35 cm/s^2, showed the high values, for example ~4.5 for DNL values. However, these indicators stayed at low level for the other aftershocks, for example ~1.5 for DNL values. We inferred from these observations that the nonlinear soil behavior vanished after the mainshock, but excited again by the slightly stronger ground motions from two aftershocks. It was very different from the above-mentioned three stations, where the disappearing nonlinear soil behavior excited by the strong mainshock ground motion did not occur during the aftershocks, even if they suffered from the strong or slightly stronger aftershock ground motion. The very soft soil at the NBSS station, class-E site, may be one main aspect for this discrepancy.

The changes of the predominant frequency with time were plotted in Fig. 10 for the ten stations. The recovery of the predominant frequency after the Kaikōura mainshock was generally observed, indicating that the soil structure recovered to the previous states before the mainshock.

6. Conclusions

In this study, the nonlinear soil behavior and its variation with time were investigated for 44 strong-motion stations during the 2016 M_w7.8 Kaikōura seismic sequence based on the S-wave H/V spectra ratio method. Differences of the H/V spectral ratio curves between the weak aftershock recordings with PGA<10 cm/s^2 and strong mainshock recordings with PGA>100 cm/s^2. Differences were represented mainly by the predominant frequency and three quantitative nonlinearity indicators, including DNL, ADNL, and PNL.

The strong ground motion during the Kaikoura mainshock brought about the significant modification to the site response at more than half of the stations considered in this study, where the nonlinearity indicators DNL, ADNL, and PNL were generally greater than 4.0, 0.3, and 10%, respectively. Meanwhile, the strong ground motions generally resulted in the shift of the predominant frequency to the lower frequency for almost all stations with identifiable predominant frequency. It was clearly found that the large strain proxy represented by PGV/V_{s30} was obtained as the nonlinearity indicators showed the high values. The deformation proxy may be a much better indicator for the occurrence of the nonlinear soil behavior given the credible shear-wave velocity was widely available.

We further focused on the variation of the nonlinear soil behavior with time at ten stations. Although the soil stepped into the nonlinearity stage due to the strong ground motion of the Kaikoura mainshock, the soil structure completely recovered during more or less time after the strong ground shaking. The relatively stronger ground motion, e.g., PGA = 30–60 cm/s^2 immediately exerted about several tens seconds after the strong ground motion played an important part in prolonging the recovery time. As the recovery completed, relatively stronger ground motion, which was not able to bring the soil into nonlinearity independently, may possess the ability to bring the soil into nonlinearity again for the very soft soil site.

Data and resources

Strong-motion recordings used in this study were derived from the GeoNet Strong Motion Data Products at https://www.geonet.org.nz (last accessed July 2019). T_{site} and V_{S30} values used in this study were derived from the New Zealand Strong Motion database of site metadata compiled by Kaiser [29] and available on the GeoNet website (https://www.geonet.org.nz/data/supplementary/nzsmdb, last accessed July 2019).

Declaration of competing interest

The authors declared that they have no conflicts of interest to this work. We declare that we do not have any commercial or associative interest that represents a conflict of interest in connection with the work submitted.

Acknowledgements

We sincerely appreciated the three anonymous reviewers for providing the valuable comments to improve the quality of this study. This work was supported by the National Key R&D Program of China (No.2017YFC1500801); National Natural Science Foundation of China (Nos. 51808514 and 51778589); Science Foundation of the Institute of Engineering Mechanics, China Earthquake Administration (No. 2018B03).

References

[1] Boore DM, Stewart JP, Seyhan E, Atkinson GM. NGA-West2 equations for predicting PGA, PGV , and 5% damped PSA for shallow crustal earthquakes. Earthq 2014;30(3):1057–85.
[2] Beresnev IA, Wen KL. Nonlinear soil response - a reality. Bull Seismol Soc Am 1996; 86(6):1964–78.
[3] Wu CQ, Peng ZG, Ben-Zion Y. Refined thresholds for non-linear ground motion and temporal changes of site response associated with medium-size earthquakes. Geophys J Int 2010;182:1567–76.
[4] Rubinstein JL. Nonlinear site response in medium magnitude earthquakes near Parkfield, California. Bull Seismol Soc Am 2011;101(1):275–86.
[5] Régnier J, Cadet H, Bonilla LF, Bertrand E, Semblat JF. Assessing nonlinear behavior of soils in seismic site response: statistical analysis on KiK-net strong-motion data. Bull Seismol Soc Am 2013;103(3):1750–70.
[6] Rubinstein JL, Beroza GC. Depth constraints on nonlinear strong ground mo-tion from the 2004 Parkfield earthquake. Geophys Res Lett 2005;32:L14313.
[7] Chandra J, Guéguen P, Steidl JH, Bonilla LF. In situ assessment of the G–γ curve for characterizing the nonlinear response of soil: application to the Garner V alley downhole array and the wildlife liquefaction array. Bull Seismol Soc Am 2015;105 (2A):993–1010.
[8] Wen KL, Chang TM, Lin CM, Chiang HJ. Identification of nonlinear site response using the H/V spectral ratio method. Terr Atmos Ocean Sci 2006;17:533–46.
[9] Beresnev IA, Wen KL. Nonlinear soil response - a reality. Bull Seismol Soc Am 1996; 86(6):1964–78.
[10] Wu CQ, Peng ZG, Dominic A. Temporal changes in site response associated with the strong ground motion of the 2004 Mw 6.6 mid-niigata earthquake sequences in Japan. Bull Seismol Soc Am 2009;99(6):3487–95.
[11] Kubo H, Nakamura T, Suzuki W, Dhakal YP, Kimura T, Kunugi T, et al. Ground-motion characteristics and nonlinear soil response observed by DONET1 seafloor observation network during the 2016 southeast off-mie, Japan, earthquake. Bull Seismol Soc Am 2019;109(3):976–86.
[12] Assimaki D, Li W, Steidl JH, Schmedes J. Quantifying nonlinearity susceptibility via site-response modeling uncertainty at three sites in the Los Angeles Basin. Bull Seismol Soc Am 2008;98(5):2364–90.
[13] Bonilla LF, Tsuda K, Pulido N, Regnier J, Laurendeau A. Nonlinear site response evidence of K-NET and KiK-net records from the 2011 off the Pacific coast of Tohoku earthquake. Earth Planets Space 2011;63:785–9.
[14] Noguchi S, Sasatani T. Quantification of degree of nonlinear site response. In: The 14th world conference on earthquake engineering, beijing, China; 2008.
[15] Régnier J, Cadet H, Bard P. Empirical quantification of the impact of nonlinear soil behavior on site response. Bull Seismol Soc Am 2016;106(4):1710–9.
[16] Ren YF, Wen RZ, Yao XX, Ji K. Five parameters for the evaluation of the soil nonlinearity during the ms8.0 wenchuan earthquake using the hvsr method. Earth Planets Space 2017;69(1):116.
[17] Kaoru S, Haruo S, Hisashi N, Takeshi N. Time-lapse changes of seismic velocity in the shallow ground caused by strong ground motion shock of the 2000Western-tottori earthquake, Japan, as revealed from coda deconvolution analysis. Bull Seismol Soc Am 2009;99(1):352–66.
[18] Chandra J, Guéguen P, Steidl JH, Bonilla LF. In situ assessment of the G–γ curve for characterizing the nonlinear response of soil: application to the Garner V alley downhole array and the wildlife liquefaction array. Bull Seismol Soc Am 2015;105 (2A):993–1010.
[19] Chandra J, Guéguen P, Bonilla LF. PGA − PGV=VSconsidered as a stress–strain proxy for predicting nonlinear soil response. Soil Dynam Earthq Eng 2016;85: 146–60.
[20] Guéguen P. Predicting nonlinear site response using spectral acceleration vs PGV=V_{s30}: a case history using the V olvi-test site. Pure Appl Geophys 2016;173 (6):2047–63.
[21] Guéguen P, Bonilla LF, Douglas J. Comparison of soil nonlinearity (in situ stress–strain relation and $G/g_{\max}$ reduction) observed in strong-motion databases and modeled in ground-motion prediction equations. Bull Seismol Soc Am 2019; 109(1):178–86.
[22] Bonilla LF, Guéguen P, Ben-Zion Y. Monitoring coseismic temporal changes of shallow material during strong ground motion with interferometry and autocorrelation. Bull Seismol Soc Am 2019;109(1):187–98.
[23] Kearse JR, an Dissen RV, Barnes P, Langridge R, Mountjoy J, Ries W, Villamor P, Clark K, Benson A, Lamarche G, et al. Onshore to offshore ground-surface and seabed rupture of the Jordan–Kekerengu–Needles fault network during the 2016, Mw7.8 Kaikōura earthquake, New Zealand. Bull Seismol Soc Am 2018;108(3B): 1573–95.
[24] Little T, an Dissen RV, Kearse J, Norton K, Wang N. Ke-kerengu fault, New Zealand: timing and size of Late Holocene surface ruptures. Bull Seismol Soc Am 2018;108 (3B).
[25] Litchfield NJ, Villamo P, V an Dissen RJ, Nicol A, Barnes PM, Barrell DJA, Pettinga J, Langridge RM, Little TA, Mountjoy J, et al. Surface rupture of multiple crustal faults in the Mw7.8 2016 Kaikōura, New Zealand, earthquake. Bull Seismol Soc Am 2018;108(3B).
[26] Bradley BA, Razafindrakoto HNT, Polak V. Ground-motion observations from the 14 november 2016 Mw 7.8 Kaikōura, New Zealand, earthquake and insights from broadband simulations. Seismol Res Lett 2017;88:1–17.
[27] Berryman K, Hamling, et al. Introduction to the special issue on the 2016 Kaikōura earthquake. Bull Seismol Soc Am 2018;108(3B):1491–5.
[28] Bradley BA, Wotherspoon LM, Kaiser AE, Cox BR, Jeong S. Influence of site effects on observed ground motions in the Wellington region from the Mw7.8 Kaikōura, New Zealand, earthquake. Bull Seismol Soc Am 2018;108(3B):1722–35.
[29] Kaiser AE, Houtte CV, Perrin ND, Wotherspoon L, Verry GHM. Site characterisation of GeoNet stations for the New Zealand strong motion database. Bull N Z Soc Earthq Eng 2017;50:39–49.
[30] Husid P. Gravity effects on the earthquake response of yielding structures. Report of earthquake engineering research laboratory. Pasadena, California: California Institute of Technology; 1967.
[31] McCann MWJ, Shah HC. Determining strong motion duration of earthquakes. Bull Seismol Soc Am 1979;69:1253–65.
[32] Hassani B, Zafarani H, Farjoodi J, Ansari A. Estimation of site amplification, attenuation and source spectra of S-waves in the East-Central Iran. Soil Dynam Earthq Eng 2011;31:1397–413.
[33] Ren YF, Wen RZ, Yamanaka H, Kashima T. Site effects by generalized inversion technique using strong motion recordings of the 2008 Wenchuan earthquake. Earthq Eng Eng Vib 2013;12:165–84.
[34] Wang HW, Ren YF, Wen RZ. Source parameters, path attenuation, and site effects from strong-motion recordings of the Wenchuan aftershocks (2008-2013) using nonparametric generalized inversion technique. Geophys J Int 2018;212:872–90.
[35] Wang HW, Ren YF, Wen RZ, Xu PB. Breakdown of earthquake self-similar scaling and source rupture directivity in the 2016-2017 central Italy seismic sequence. J Geophys Res: Solid Earth 2019;124(4):3898–917.
[36] Konno K, Ohmachi T. Ground-motion characteristics estimated from ratio between horizontal and vertical components of microtremor. Bull Seismol Soc Am 1998;88: 228–41.
[37] Nakamura Y. A method for dynamic characteristics estimation of subsurface using microtremor on the ground surface. QR of RTR1 1989;30:1. February.
[38] Noguchi S, Sasatani T. Quantification of degree of nonlinear site response. In: The 14th world conference on earthquake engineering, beijing, China; 2008.
[39] Drnevich VP, Fe Richart Jr. Dynamic prestraining of dry sand. J Soil Mech Found Div 1970;96(2):453–69. 1970.
[40] Dobry R, Ladd R. Discussion of "Soil liquefaction and cyclic mobility evaluation for level ground during earthquakes," by Seed H.B. and "Liquefaction potential: Science versus practice," by Peck R.B. J Geotech Eng Div 1980;106(6):720–4.
[41] Youd TL. Compaction of sands by repeated shear straining. J. Soil Mech Found Eng Div. 1972;98(7):709–25.
[42] Vucetic M. Cyclic threshold shear strains in soils. J. Geotech Eng. 1994;120: 2208–28.